Wataru Ohnishi, Thomas Beauduin, Hiroshi Fujimoto: Preactuated Multirate Feedforward Control for Independent Stable Inversion of Unstable Intrinsic and Discretization Zeros, IEEE/ASME Transactions on Mechatronics, Vol. 24, No.2, pp. 863-871, 2019. https://doi.org/10.1109/TMECH.2019.2896237

Preactuated Multirate Feedforward Control for Independent Stable Inversion of Unstable Intrinsic and Discretization Zeros

Wataru Ohnishi, *Member, IEEE,* Thomas Beauduin, *Member, IEEE,* and Hiroshi Fujimoto, *Senior Member, IEEE*

***Abstract*—A plant with unstable zeros is known to be difficult to be controlled, because of the initial undershoot of its step response and the unstable poles in its inversion system. There are two reasons why a plant has unstable zeros in the discrete time domain: 1) non-collocation of actuators and sensors, 2) discretization by zero-order hold. Addressing problems 1) and 2) simultaneously, approximate and discrete-time stable inversion methods have been proposed as model-based feedforward control for unstable zeros. However, the approximated inversion methods compromise tracking performance, and the discrete-time stable inversion methods obtain oscillatory control inputs owing to the direct cancellation of discretization zeros. Therefore, this paper proposes a preactuated multirate feedforward control, which is an independent stable inversion of the two types of zeros: unstable intrinsic zeros from non-collocation and unstable discretization zeros from the zero-order hold. The proposed method combines both a state trajectory generation based on a time and imaginary axis reversal to address problem 1), and a multirate feedforward implementation to address problem 2), independently. Moreover, this study verifies the tracking performance improvement by performing simulations and experiments in comparison with well-known model-based feedforward control methods using a high-precision motion stage. The role and importance of multirate feedforward control are also demonstrated by comparing it to a continuous-time domain approach with preactuation.**

***Index Terms*—Preactuation, Multirate feedforward, Non-minimum phase system, Unstable zero, Discretization**

I. Introduction

TRACKING control with zero gain and phase errors between the desired and output trajectories at every sampling point can be achieved, in theory, by model inversion (i.e., pole-zero cancellation). However, a plant with unstable (i.e., non-minimum phase, NMP) zeros gives rise to an initial undershoot when stepped (Fig. 1) and highly oscillatory or unstable control trajectories when inverted [1], [2]. Unstable zeros of discrete transfer functions can be classified as 1) intrinsic zeros corresponding to the plant dynamics (e.g., non-collocated placement of sensor and actuator) or 2) discretization zeros due to signal sampling [3]. Note that discretization zeros are unstable when the relative order of the continuous time plant is greater than two, even without continuous-time unstable zeros [4]. Systems with unstable zeros are, for instance, wafer stages [5], high-precision positioning stages for flat panel display manufacturing systems [6], [7], hard disk drives [8], boost converters [9], permanent magnet synchronous motors during six-step operation [10], backward driving cars [11], and pitch angle regulation of aircraft [12].

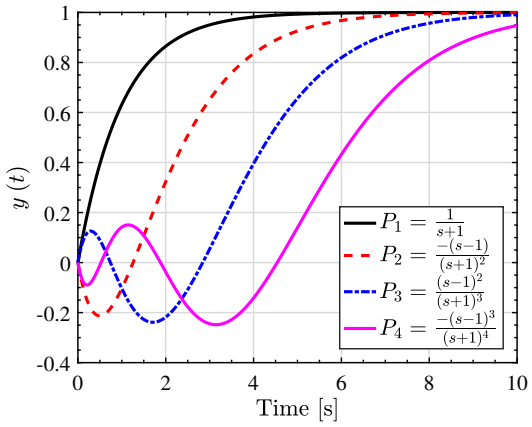

Fig. 1. Step response comparison: P_1 is a first order transfer function without an unstable zero. P_2, P_3, and P_4 have one, two, and three unstable zero(s), respectively

Extensive research has been dedicated to the design of tracking control methods for systems with NMP zeros. The existing proposals can be classified as (i) approximate model-inversion methods and (ii) preactuated model inversion methods [13]. A straightforward way to implement an approximate inversion is to cancel stable poles and zeros while ignoring NMP zeros, i.e., NPZI-method [14]. This approach exhibits both magnitude and phase errors; hence, zero-magnitude-error tracking control (ZMETC) [15] and zero-phase-error tracking control (ZPETC) [16] methods have been proposed and improved upon. Despite the stable control input, NPZI, ZMETC, and ZPETC may not yield satisfactory tracking performance owing to the approximations involved (depending on the system and performance specifications).

Preactuated model inversion can achieve perfect tracking with infinite preview (i.e., knowledge of future references) and preactuation (i.e., actuation applied a time-interval before the actual output of the system). Continuous-time domain stable inversion methods are proposed in [17], [18], [19], [20]. This study unifies these proposals as CPMI or continuous-time preactuated model-inverse methods. However, these approaches do not consider the effect of the zero-order hold. There lays the key difference between the CPMI method and the proposed preactuated multirate feedforward control, which explicitly

The authors are with the University of Tokyo, 7-3-1 Hongo, Bunkyo-ku, Tokyo, 113-8656, Japan (e-mail: ohnishi@ieee.org; thomas.beauduin15@ae.k.u-tokyo.ac.jp; fujimoto@k.u-tokyo.ac.jp).

Manuscript received April 19, 2005; revised August 26, 2015.

considers the effect of the zero-order hold by constructing a multirate system. Alternatively, a discrete-time domain approach is proposed in [21], which compensates both intrinsic and discretization unstable zeros, simultaneously. This method can achieve perfect tracking at each sampling point, but it can cause high oscillations in the inter-sampling behavior by direct cancellation of the discretization zeros [1], [22]. For high-precision motion systems such as wafer scanners and printing systems, preactuation methods have been proposed and applied, focusing on iterative learning control and linear periodically time-varying (LPTV) systems [23], [24].

We propose a multirate feedforward with preactuation [25] and experimentally validate its effectiveness [26]. The proposed method solves problems 1) and 2) independently, regardless of the desired trajectory given it is $n-1$ differentiable (where n denotes the order of the nominal plant). This paper concludes our findings and provides an in-depth review and comparison of the effectiveness of the independent inversion with a wide range of established techniques in the field.

First, the unstable intrinsic zeros in the continuous time domain are offset through a state trajectory generation using a time-axis reversal. Then, the stable inversion of the discretization zeros is calculated through a multirate feedforward approach [27]. Note that the multirate control is commonly referred to as the set of techniques used to improve *feedback* control performance [28], [29], [30]. These methods use multiple sampling times to enhance the performance/cost trade-off present in single-rate feedback control. In contrast, this multirate method is for model-based *feedforward* control, using multiples of the sampling time to obtain a stable inversion of the discretization zeros. A multirate *feedforward* method is proposed in [27] and extended to systems with continuous-time stable zeros [7] and adaptive control [31]. Reference [8] proposed a multirate NPZI method, which ignores only intrinsic (continuous time) unstable zeros, whereas the single-rate NPZI method introduced in III-A and [14] ignores both intrinsic and discretization zeros simultaneously. This method [8] constructs a stable inversion of the discretization zeros; however, it is still affected by the approximation of the unstable intrinsic zeros. The proposal described in this paper goes a step further, improving upon the model inversion and subsequently tracking errors of systems with non-minimum phase zeros. It is an independent stable inversion for unstable intrinsic zeros and discretization zeros, which are inverted by preactuation and multirate feedforward, respectively.

To demonstrate the effectiveness, this paper thoroughly compares the proposed method with both approximate and preactuated model inversion methods by simulations and experiments. This paper shows that it is impossible to compensate for the zero-order hold delay by only previewing the reference of CPMI method. The considered system has several intrinsic and discretization unstable zeros for which conventional approximate methods are unable to achieve perfect tracking. Simulation and experimental results show that the proposed method effectively reduces tracking errors. Note that the performance of model-based methods including the proposed method is affected by modeling errors, which can be mitigated by feedback control. However, because of the presence of continuous time unstable zeros in the lower frequency range, it is difficult to design high-bandwidth feedback controllers. Hence, for a system with unstable zeros, precise system identification inherently plays a crucial role. Albeit, for the range of applications targeted, extensive modeling and identification are at present commonly employed.

II. Notations and definitions

The plant in continuous time domain is defined as $P_c(s)$. $P_s[z_s]$ denotes the discretized plant of $P_c(s)$ by the zero-order hold with sampling time T_u, where s denotes a complex variable for Laplace transform and $z_s = e^{T_u s}$.

A continuous-time transfer function of the nominal plant is

$$P_n(s) = \frac{B(s)}{A(s)}, \tag{1}$$

where $A(s)$ is nth order and $B(s)$ mth order

$$\begin{aligned} A(s) &= \frac{s^n + a_{n-1}s^{n-1} \cdots + a_0}{b_0} \\ B(s) &= \frac{b_m s^m + b_{m-1}s^{m-1} + \cdots + b_0}{b_0}. \end{aligned} \tag{2}$$

Note that (1) is irreducible. The state and output equations of (1) are defined as

$$\dot{\boldsymbol{x}}(t) = \boldsymbol{A}_c\boldsymbol{x}(t) + \boldsymbol{b}_c u(t), y(t) = \boldsymbol{c}_c\boldsymbol{x}(t). \tag{3}$$

The discretized plant by a zero-order hold with sampling time T_u is defined as

$$\boldsymbol{x}[k+1] = \boldsymbol{A}_s\boldsymbol{x}[k] + \boldsymbol{b}_s u[k],\ \ y[k] = \boldsymbol{c}_s\boldsymbol{x}[k] \tag{4}$$

$$\boldsymbol{A}_s = e^{\boldsymbol{A}_c T_u},\ \ \boldsymbol{b}_s = \int_0^{T_u} e^{\boldsymbol{A}_c\tau} d\tau \cdot \boldsymbol{b}_c,\ \ \boldsymbol{c}_s = \boldsymbol{c}_c. \tag{5}$$

In the discrete transfer function, it is defined as

$$P_n[z_s] = \boldsymbol{c}_s(z_s\boldsymbol{I} - \boldsymbol{A}_s)^{-1}\boldsymbol{b}_s. \tag{6}$$

III. Single-rate Model-Inversion methods

A. Approximate Model-Inverse Methods

When a nominal plant $P_n[z_s]$ discretized by zero-order hold has an unstable zero, the inversion system in the feedforward controller $P_n^{-1}[z_s]$ becomes unstable. To avoid this problem, several approximate model-inverse feedforward controllers $\tilde{P}_n^{-1}[z_s]$ have been proposed in the literature. A generalized block diagram is shown in Fig. 2 in which T_y and T_u denote the sampling and control periods, respectively. In this section, $T_y = T_u$ because only single-rate ($z_s = e^{T_u s}$) control methods are considered. Approximations decompose the nominal plant in a stable $B^{\mathrm{st}}[z_s]$ and unstable part, $B^{\mathrm{ust}}[z_s]$

$$P_n[z_s] = \frac{B[z_s]}{A[z_s]} = \frac{B^{\mathrm{st}}[z_s]B^{\mathrm{ust}}[z_s]}{A[z_s]} \tag{7}$$

$$B^{\mathrm{ust}}[z_s] = b_{un_u}z_s^{n_u} + b_{u(n_u-1)}z_s^{n_u-1} + \cdots + b_{u0}, \tag{8}$$

where n_u denotes the order of $B^{\mathrm{ust}}[z_s]$. The feedforward controller is then designed as

$$C_{ff}[z_s] = \tilde{P}_n^{-1}[z_s] = \frac{z_s^{-q}A[z_s]}{B^{\mathrm{st}}[z_s]\tilde{B}^{\mathrm{ust}}[z_s]}. \tag{9}$$

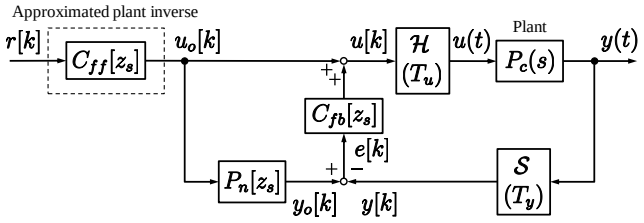

Fig. 2. Approximated plant inverse feedforward control configuration, where $C_{ff}[z_s] = \tilde{P}_n^{-1}[z_s]$. $\tilde{P}_n[z_s]$ is the approximated nominal plant model without unstable zeros. $P_c(s)$ and $C_{fb}[z_s]$ denote the continuous time plant and discrete time feedback controller, respectively. $\mathcal{H}$ and $\mathcal{S}$ denote a holder and a sampler, respectively.

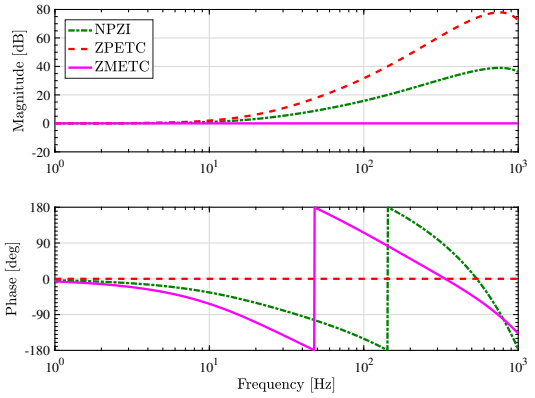

Fig. 3. Example of tracking control performance of single-rate model-inversion methods $C_{ff}[z_s]P_s[z_s]z_s^{n_{pre}}$, where n_{pre} denotes the previewed number of samples for ZPETC. The plant shown in Fig. 6(b) is used for the case study.

The difference between the three prominent methods (NPZI, ZPETC and ZMETC) is the design of $\tilde{B}^{\mathrm{ust}}[z_s]$ and q ($0 \leq q \in \mathbb{Z}$). Please refer to Reference [14] for an overview. A Bode plot of tracking control performances of single-rate model-inversion methods is shown in Fig. 4, where a plant shown in Fig. 6(b) is used as a case study.

B. Continuous-time Preactuated Model-Inverse methods

Several continuous-time preactuated model-inverse (CPMI) methods are proposed in [17], [18], [19], [20]. However, these papers do not consider the effect of the zero-order hold. The key difference between CPMI methods and the proposed method is the zero-order hold consideration by multirate feedforward control. A block diagram of CPMI method is shown in Fig. 4.

1) Step 1: Stable-unstable decomposition: $B(s)^{-1}$ defined in (2) is decomposed into a stable part $F^{\mathrm{st}}(s)$ and an unstable part $F^{\mathrm{ust}}(s)$ as follows:

$$B(s)^{-1} = \frac{b_0}{b_m s^m + b_{m-1}s^{m-1} + \cdots + b_0} \tag{10}$$

$$= F^{\mathrm{st}}(s) + F^{\mathrm{ust}}(s), \tag{11}$$

$$f^{\mathrm{st}}(t) = \mathcal{L}^{-1}\left[F^{\mathrm{st}}(s)\right], \bar{f}^{\mathrm{ust}}(t) = \mathcal{L}^{-1}\left[F^{\mathrm{ust}}(-s)\right], \tag{12}$$

where $\mathcal{L}^{-1}$ denotes the inverse uni-lateral Laplace transform. Note that $F^{\mathrm{ust}}(-s)$ is stable.

2) Step 2: Stable part feedforward control input: Stable part feedforward control input is calculated by a convolution between the reference $\boldsymbol{A}_{\mathrm{CPMI}}\boldsymbol{r}_{\mathrm{CPMI}}(t)$ and $f^{\mathrm{st}}(t)$.

$$u_{ff}^{\mathrm{st}}(t) = \int_{-\infty}^{t} f^{\mathrm{st}}(t-\tau)\boldsymbol{A}_{\mathrm{CPMI}}\boldsymbol{r}_{\mathrm{CPMI}}(\tau)d\tau, \tag{13}$$

where

$$\begin{aligned}\boldsymbol{A}_{\mathrm{CPMI}} &= \frac{1}{b_0}\begin{bmatrix}a_0 & a_1 & \cdots & a_{n-1} & 1\end{bmatrix}\\ \boldsymbol{r}_{\mathrm{CPMI}} &= \begin{bmatrix}1 & \rho & \cdots & \rho^n\end{bmatrix}^{\mathrm{T}} r(t),\end{aligned} \tag{14}$$

where ρ denotes the Heaviside operator [33]. Equation (13) can be written as

$$u_{ff}^{\mathrm{st}}(t) = \int_{0}^{t} f^{\mathrm{st}}(t-\tau)\boldsymbol{A}_{\mathrm{CPMI}}\boldsymbol{r}_{\mathrm{CPMI}}(\tau)d\tau, \tag{15}$$

assuming $\boldsymbol{r}_{\mathrm{CPMI}}(t) = \boldsymbol{0}$ when $t < 0$.

3) Step 3: Unstable part feedforward control input: Unstable part feedforward control input is calculated by 1) a convolution between the time axis reversed reference $\boldsymbol{A}_{\mathrm{CPMI}}\boldsymbol{r}_{\mathrm{CPMI}}(-\bar{\tau})$ and the stable signal $\bar{f}^{\mathrm{ust}}(\bar{t}-\bar{\tau})$ and 2) a time axis reversal. This procedure results in an infinity time preactuation for continuous-time unstable zeros compensation.

$$u_{ff}^{\mathrm{ust}}(t) = \int_{-\infty}^{\bar{t}} \bar{f}^{\mathrm{ust}}(\bar{t}-\bar{\tau})\boldsymbol{A}_{\mathrm{CPMI}}\boldsymbol{r}_{\mathrm{CPMI}}(-\bar{\tau})d\bar{\tau}\Big|_{\bar{t}=-t} \tag{16}$$

4) Step 4: Total feedforward control input: Total feedforward control input is calculated by a sum of the stable and the unstable part feedforward control input.

$$u_o(t) = u_{ff}^{\mathrm{st}}(t) + u_{ff}^{\mathrm{ust}}(t) \tag{17}$$

Then $u_{ff}(t)$ is sampled into $u_{ff}[k]$ by a zero-order hold. No consideration of the zero-order hold causes a delay. This will be discussed in section V-F and shown in Fig. 11.

IV. Preactuated Multirate Feedforward Control

We propose a multirate feedforward control with preactuation to design a stable inversion feedforward controller for plants with unstable intrinsic and discretization zeros. This method solves the unstable zeros inversion problem in three steps. First, we calculate the controllable canonical form realization for the nominal plant. Second, the stable inversion for the unstable intrinsic zeros is calculated using a time axis reversal and imaginary axis reversal in a continuous time domain. Then, stable inversion for unstable discretization zeros is calculated using a multirate feedforward proposed by [27]. A block diagram of the preactuated multirate feedforward control is shown in Fig. 5.

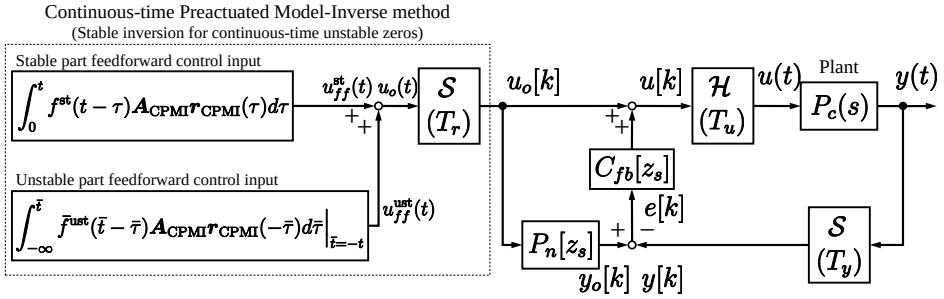

Fig. 4. Continuous-time Preactuated Model-Inverse method. The stable inversion of the continuous time plant is calculated thorough the dotted boxed blocks. Note that this step does not consider the zero-order hold of the plant.

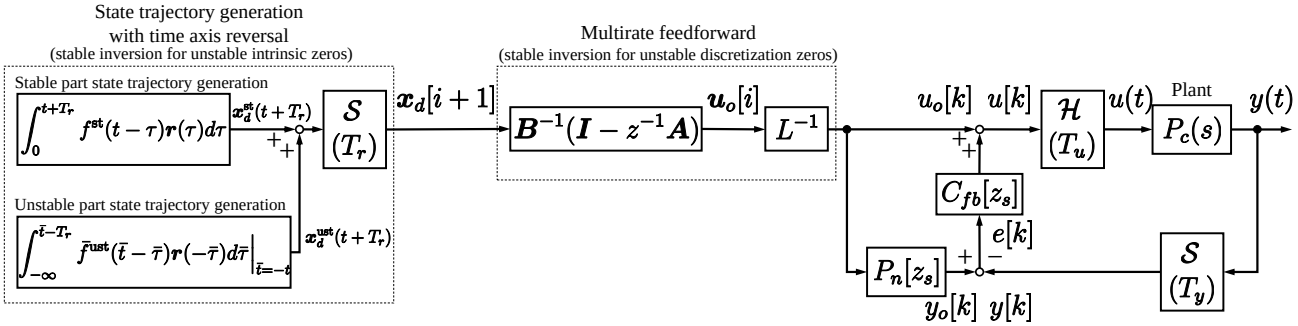

Fig. 5. Proposed preactuated multirate feedforward control. $\mathcal{S}$, $\mathcal{H}$, and L denote a sampler, holder, and lifting operator [32], respectively. z and z_s denote e^{sT_r} and e^{sT_u}, where $T_r = nT_u$, respectively.

A. Controllable canonical form realization

We realize the nominal plant shown in (3) as the controllable canonical form:

$$\begin{aligned}
\boldsymbol{x}(t) &= \begin{bmatrix} x_1(t) & x_2(t) & \cdots & x_n(t) \end{bmatrix}^{\mathrm{T}}, \\
\boldsymbol{A}_c &= \begin{bmatrix} 0 & 1 & 0 & \cdots & 0 \\ 0 & 0 & 1 & \cdots & 0 \\ & & & \ddots & \\ -a_0 & -a_1 & -a_2 & \cdots & -a_{n-1} \end{bmatrix} \\
\boldsymbol{b}_c &= \begin{bmatrix} 0 & 0 & \cdots & b_0 \end{bmatrix}^{\mathrm{T}}, \\
\boldsymbol{c}_c &= \begin{bmatrix} 1 & \frac{b_1}{b_0} & \cdots & \frac{b_m}{b_0} & 0 & \cdots & 0 \end{bmatrix}.
\end{aligned} \tag{18}$$

The objective to use the controllable canonical form is to use the differential relationship of the state vector as shown in (20).

B. State trajectory $\boldsymbol{x}_d$ generation

First, a desired state trajectory $\boldsymbol{x}_d$ for the multirate feedforward is generated. The state trajectory $\boldsymbol{x}_d$ is defined as

$$\boldsymbol{x}_d(t) = \begin{bmatrix} x_{1d}(t) & x_{2d}(t) & \cdots & x_{nd}(t) \end{bmatrix}^{\mathrm{T}}. \tag{19}$$

Owing to the controllable canonical form realization (see (18)),

$$\boldsymbol{x}_d(t) = \begin{bmatrix} x_{1d}(t) & \rho x_{1d}(t) & \cdots & \rho^{n-1} x_{1d}(t) \end{bmatrix}^{\mathrm{T}}. \tag{20}$$

According to (3), to track the reference position trajectory $r(t)$, the desired state trajectory $\boldsymbol{x}_d(t)$ should satisfy

$$\begin{aligned}
r(t) &= \boldsymbol{c}_c \boldsymbol{x}_d(t) \\
&= \begin{bmatrix} 1 & \frac{b_1}{b_0} & \cdots & \frac{b_m}{b_0} & 0 & \cdots & 0 \end{bmatrix} \begin{bmatrix} x_{1d}(t) \\ \rho x_{1d}(t) \\ \rho^2 x_{1d}(t) \\ \vdots \\ \rho^{n-1} x_{1d}(t) \end{bmatrix}.
\end{aligned} \tag{21}$$

From (21) and (2), $x_{1d}(t)$ is obtained by

$$x_{1d}(t) = \frac{1}{B(\rho)} r(t). \tag{22}$$

Therefore, the entire vector $\boldsymbol{x}_d(t)$ is obtained by

$$\boldsymbol{x}_d(t) = \frac{1}{B(\rho)} \boldsymbol{r}(t), \tag{23}$$

where

$$\begin{aligned}
\boldsymbol{r}(t) &= \begin{bmatrix} r_1(t) & r_2(t) & \cdots & r_n(t) \end{bmatrix}^{\mathrm{T}} \\
&= \begin{bmatrix} 1 & \rho & \cdots & \rho^{n-1} \end{bmatrix}^{\mathrm{T}} r(t).
\end{aligned} \tag{24}$$

However, (23) has unstable poles when the plant $P_n(s)$ has unstable zeros. To prevent the diversion of the state trajectory $\boldsymbol{x}_d(t)$, the stable-unstable decomposition and time axis reversal techniques are applied.

1) Step 1: Stable-unstable decomposition: Stable-unstable composition is performed as same as the CPMI method shown in the section III-B1:

$$B(s)^{-1} = \frac{b_0}{b_m s^m + b_{m-1}s^{m-1} + \cdots + b_0} \tag{25}$$
$$= F^{\mathrm{st}}(s) + F^{\mathrm{ust}}(s), \tag{26}$$
$$f^{\mathrm{st}}(t) = \mathcal{L}^{-1}\left[F^{\mathrm{st}}(s)\right], \bar{f}^{\mathrm{ust}}(t) = \mathcal{L}^{-1}\left[F^{\mathrm{ust}}(-s)\right]. \tag{27}$$

2) Step 2: Stable part state trajectory generation: The desired state trajectory $\boldsymbol{x}_d^{\mathrm{st}}(t)$ for the stable part is forwardly generated as follows.

$$\boldsymbol{x}_d^{\mathrm{st}}(t) = \begin{bmatrix} x_{1d}^{\mathrm{st}}(t) & x_{2d}^{\mathrm{st}}(t) & \cdots & x_{nd}^{\mathrm{st}}(t) \end{bmatrix}^{\mathrm{T}} = \int_{-\infty}^{t} f^{\mathrm{st}}(t-\tau)\boldsymbol{r}(\tau)d\tau \tag{28}$$

Equation (28) can be written as

$$\boldsymbol{x}_d^{\mathrm{st}}(t) = \int_{0}^{t} f^{\mathrm{st}}(t-\tau)\boldsymbol{r}(\tau)d\tau, \tag{29}$$

assuming $\boldsymbol{r}(t) = \boldsymbol{0}$ when $t < 0$.

3) Step 3: Unstable part state trajectory generation: The desired state trajectory $\boldsymbol{x}_d^{\mathrm{ust}}(t)$ for the unstable part is generated by

$$\boldsymbol{x}_d^{\mathrm{ust}}(t) = \begin{bmatrix} x_{1d}^{\mathrm{ust}}(t) & x_{2d}^{\mathrm{ust}}(t) & \cdots & x_{nd}^{\mathrm{ust}}(t) \end{bmatrix}^{\mathrm{T}} = \int_{-\infty}^{\bar{t}} \bar{f}^{\mathrm{ust}}(\bar{t}-\bar{\tau})\boldsymbol{r}(-\bar{\tau})d\bar{\tau}\Big|_{\bar{t}=-t}. \tag{30}$$

$\boldsymbol{x}_d^{\mathrm{ust}}(t)$ is calculated as follows: first, a convolution of the time reversed reference position trajectory $\boldsymbol{r}(-\bar{t})$ and the stable signal $\bar{f}^{\mathrm{ust}}(\bar{t})$ is calculated. Next, the time axis is reversed. The mathematical proof is provided in [34].

4) Step 4: State trajectory generation: The state trajectory $\boldsymbol{x}_d(t)$ is obtained by

$$\boldsymbol{x}_d(t) = \boldsymbol{x}_d^{\mathrm{st}}(t) + \boldsymbol{x}_d^{\mathrm{ust}}(t). \tag{31}$$

C. Feedforward input generation from the state trajectory

The effect of unstable discretization zeros can be avoided using the multirate feedforward control [27]. Fig. 5 shows that there are three time periods T_y, T_u, and T_r denoting the periods for $y(t)$, $u(t)$, and $r(t)$, respectively. These periods are set as $T_r = nT_u = nT_y$.

The multirate system of (4) is given as

$$\boldsymbol{x}[i+1] = \boldsymbol{A}\boldsymbol{x}[i] + \boldsymbol{B}\boldsymbol{u}[i], \ y[i] = \boldsymbol{c}\boldsymbol{x}[i], \tag{32}$$

where

$$\boldsymbol{A} = \boldsymbol{A}_s^n, \ \boldsymbol{B} = \begin{bmatrix} \boldsymbol{A}_s^{n-1}\boldsymbol{b}_s & \boldsymbol{A}_s^{n-2}\boldsymbol{b}_s & \cdots & \boldsymbol{A}_s\boldsymbol{b}_s & \boldsymbol{b}_s \end{bmatrix}$$
$$\boldsymbol{c} = \boldsymbol{c}_s, \ \boldsymbol{x}[i] = \boldsymbol{x}(iT_r) \tag{33}$$

by calculating the state transition from $t = iT_r = kT_u$ to $t = (i+1)T_r = (k+n)T_u$. Here, the input vector $\boldsymbol{u}[i]$ is defined in the lifting form

$$\boldsymbol{u}[i] = \begin{bmatrix} u_1[i] & u_2[i] & \cdots & u_n[i] \end{bmatrix}^{\mathrm{T}} = \begin{bmatrix} u(kT_u) & u((k+1)T_u) & \cdots & u((k+n-1)T_u) \end{bmatrix}^{\mathrm{T}}. \tag{34}$$

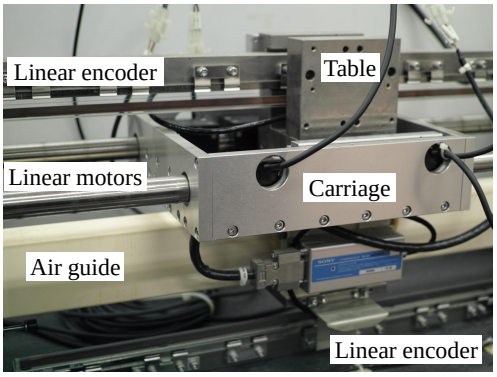

(a) High-precision positioning stage.

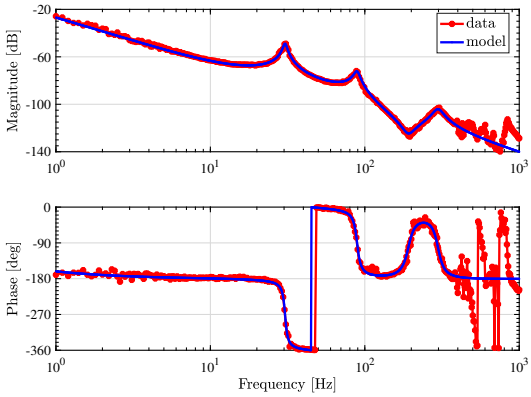

(b) FRF data and model of (a).

Fig. 6. Experimental high-precision positioning stage and its frequency response function (FRF) data and 8th order model ($L_m = 0.300$ [m]).

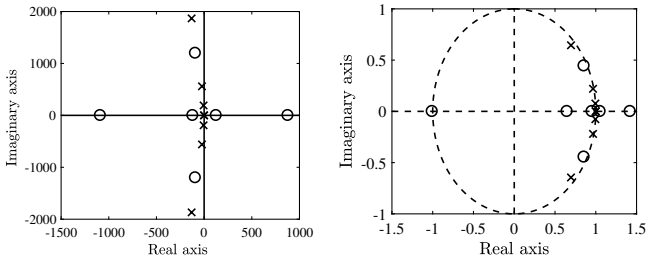

(a) P_c. (b) P_s.

Fig. 7. Pole-zero map of identified model shown in Fig. 6.

According to (32), the feedforward input $\boldsymbol{u}_o[i]$ is obtained from the previewed state trajectory $\boldsymbol{x}_d[i+1]$ as follows:

$$\boldsymbol{u}_o[i] = \boldsymbol{B}^{-1}(\boldsymbol{I} - z^{-1}\boldsymbol{A})\boldsymbol{x}_d[i+1], \tag{35}$$

where $z = e^{sT_r}$.

V. Experimental Validation

A. Experimental setup

The experimental setup used to verify the proposed theory is shown in Fig. 6. It is an air-guided single degree-of-freedom flexible stage driven by a set of linear motors. The position of the table and the driven carriage are measured by two linear encoders with 1 nm precision. By using interior or exterior division, we can measure any vertical imaginary position. In this paper, the height of the measurement point is set as $L_m = 0.300$[m] by exterior division to have continuous time unstable zeros. The applied force, i.e. current, is measured through an

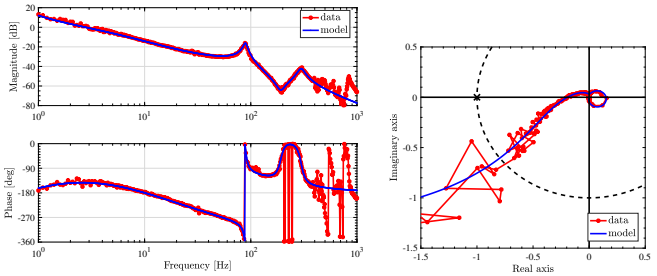

(a) Bode plot of the open loop system. (b) Nyquist plot of the open loop system.

Fig. 8. Feedback control performance. The feedback controller is designed as a PID controller and a second order shaping filter. The designed gain and phase margins are 14.2 dB (at 10 Hz) and 37.2 deg (at 2.8 Hz), respectively.

inductive current sensor with a 25 A range and quantized with a 14-bit A/D converter, i.e., 3.05 mA step.

B. System identification

The dominant system dynamics of the setup are modeled through frequency domain identification techniques; see [35]. First, the non-parametric frequency response is measured from open-loop experiments using periodic multisine excitations with quasi-logarithmic spacing to cover the wide frequency band-of-interest. Subsequently, an 8th order parametric transfer function model $P_n(s)$ is estimated iteratively using a Levenberg-Marquardt method with a maximum likelihood criterion. Some additional weighting is applied in the middle frequency range (10 to 400 Hz) to reflect the region in which high model accuracy is desired for feedforward design.

The measured frequency response and the estimated 8th order model are shown in Fig. 6(b). The identified continuous time pole-zero map is shown in Fig. 7(a), in which $P_n(s)$ contains continuous time unstable zeros at $s = +126,\ +878$ and stable zeros at $s = -1090,\ -120, -92.7 \pm 1.20j$. Additionally, the pole-zero map of the discretized transfer function with $T_u = 400\ [\mu\text{s}]$ is shown in Fig. 7(b), in which $P_s[z_s]$ contains an unstable discretization zero.

C. Conditions

The setup has a current controller as inner loop, which has a 1 kHz bandwidth, with a 12.5 kHz sampling and a position controller as outer loop with 2.5 kHz sampling. The position feedforward controllers are designed with $T_u = 400\ [\mu\text{s}]$ sampling time. The position feedback controller is designed as a proportional-integral-derivative (PID) controller and a second order shaping filter. The feedback control performance is shown in Fig. 8, which shows that it is difficult to achieve high bandwidth for a plant with continuous time unstable zeros in the low frequency range. This indicates that the feedback controller cannot help the trajectory tracking performance. The block diagram shown in Fig. 2 is used for NPZI, ZPETC, and ZMETC methods. Note that in the configurations of Fig. 2 and 5, without modeling error or disturbances, the output of the feedback controller $C_{fb}[z_s]$ is zero.

The target trajectory is given as a 0.05 second step reference interpolated by a 15th order polynomial and is shown in i.e. Fig. 9(a). As for the CMPI and the proposed methods, the control input is applied from $t = -0.0428\,[\text{s}]$ to preactuate the system. This time length is determined by the current sensor resolution. This is 5.38 times longer than the time constant of the dominant unstable zero in continuous time domain. The effect regarding short time preactuation compared to the time constant of the unstable zeros is discussed in [36].

D. Simulation results

Simulation results are shown in Fig. 9. Fig. 9(f) demonstrates that the proposed method can achieve perfect tracking without any undershoot or overshoot. In contrast, Fig. 9(a) and 9(e) show that the NPZI, ZMETC, and ZPETC controllers create undershoot and/or overshoot. The FB only case shows a slow response, which demonstrates that a plant with a slow continuous unstable zero cannot rely on a FB controller only for reference tracking. Fig. 10(g) shows that the CMPI method creates a similar current reference to the proposed method. However, due to the lack of considering the zero-order hold, the current reference is delayed compared to the proposal and it results in the tracking error shown in Fig. 9(f). Note that these simulations contain no modeling error and/or disturbances, hence, the FB current is zero for NPZI, ZPETC, ZMETC, CMPI and the proposed method.

E. Experimental results

The experimental results are shown in Fig. 10. The trend in the experimental results are in good agreement with the simulations shown in Fig. 9. From Fig. 10(e) and 10(g), during preactuation, the output position has almost no motion. After preactuation, the proposed method has almost no undershoot or overshoot. As summarized in Table I, the proposed method is experimentally validated.

Fig. 10(d) and 10(h) show that, except the FB only case, the feedback current references are quite small compared to the feedforward current references. This is because the nominal output $y_o[k]$, which is calculated by the feedforward current reference $u_o[k]$ and the nominal plant $P_n[z_s]$, almost matches the actual output $y[k]$ due to the well identified nominal model.

F. Observations of the effect of multirate feedforward

As described above, the feedforward current reference is similar between the CPMI method and the proposed method as shown in Fig. 9(g) and 10(g). The difference of the two methods is the zero-order hold consideration by the multirate feedforward.

Fig. 11 shows that tracking error comparison between the proposed method and shifted CPMI methods. It shows that the zero-order hold delay cannot be compensated by just shifting the current reference even by a non-integer sample shift. These results clearly show the importance of multirate feedforward control, which compensates for the zero-order hold delay. Fig. 11(c) shows that perfect tracking is achieved by the proposed method for every $T_r = nT_u$.

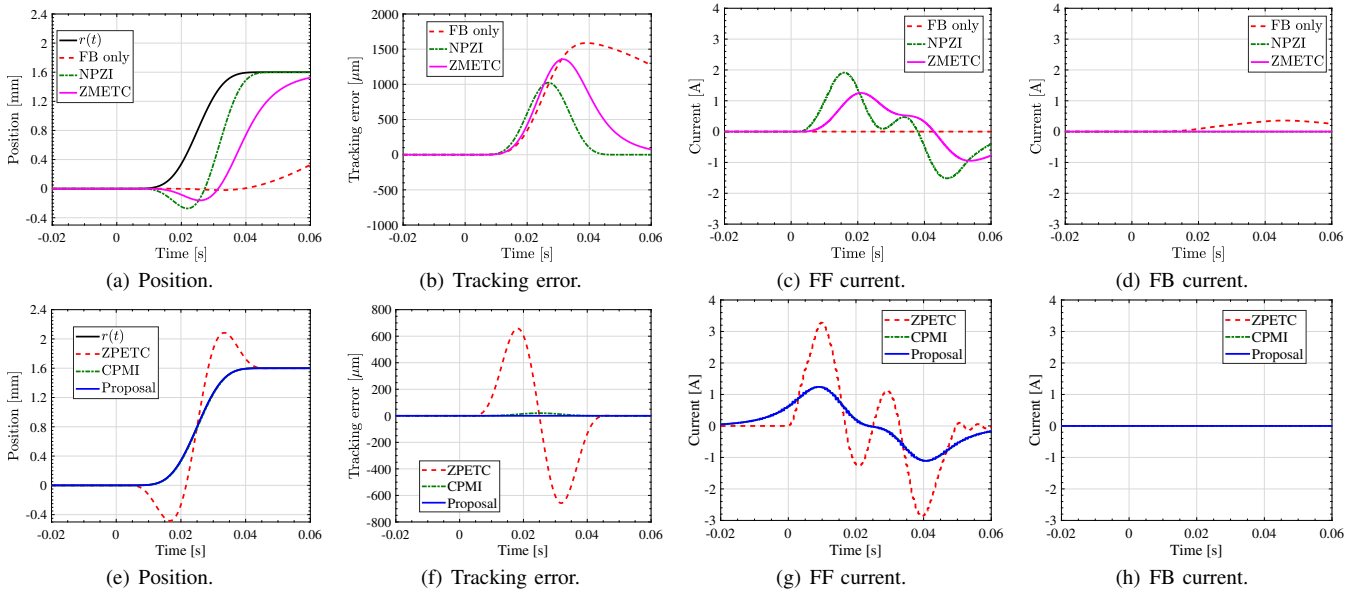

(a) Position. (b) Tracking error. (c) FF current. (d) FB current.

(e) Position. (f) Tracking error. (g) FF current. (h) FB current.

Fig. 9. Simulation with 8th order model shown in Fig. 6(b). Note that in (d) and (h), FB current is zero for NPZI, ZPETC, ZMETC, CPMI, and the proposal due to no modeling error and disturbance assumption.

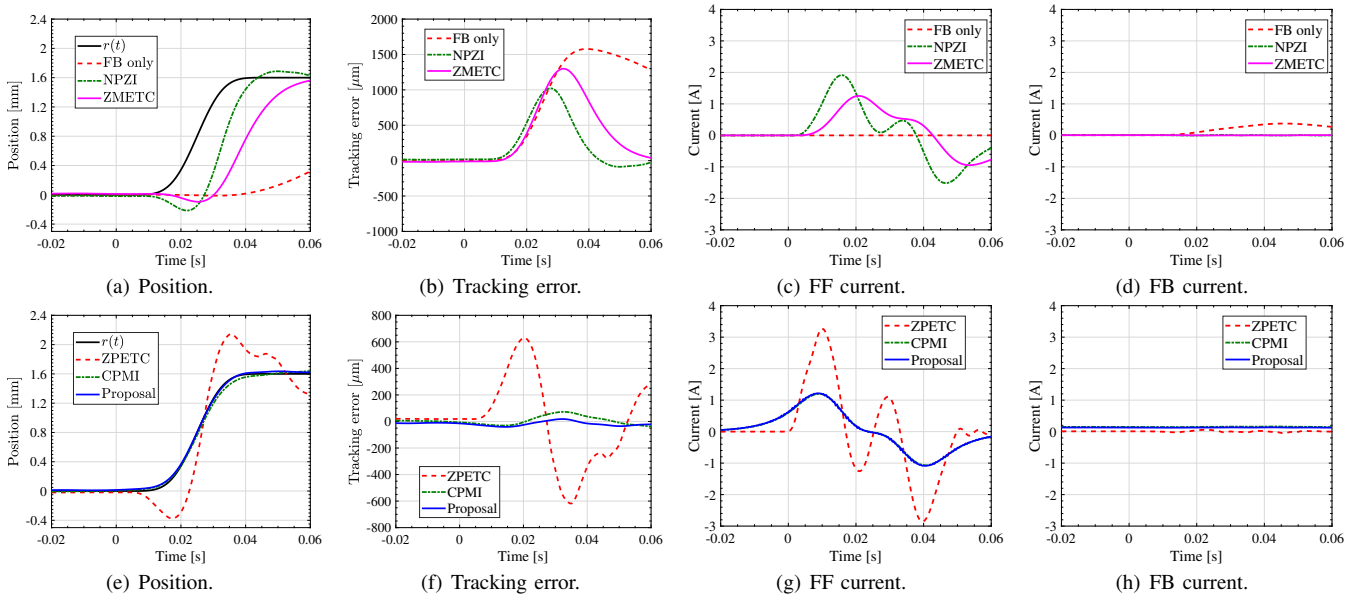

(a) Position. (b) Tracking error. (c) FF current. (d) FB current.

(e) Position. (f) Tracking error. (g) FF current. (h) FB current.

Fig. 10. Experiment with the stage shown in Fig. 6. 8th order nominal model is used for feedforward controller design.

TABLE I
MAXIMUM TRACKING ERROR IN μm OF FIGS. 9 AND 10.

	FB only	NPZI	ZMETC	ZPETC	CPMI	Proposal
Sim	1590	1020	1360	658	20.0	0.00475*
Exp	1580	1020	1300	631	72.3	41.1

* Intersample tracking error

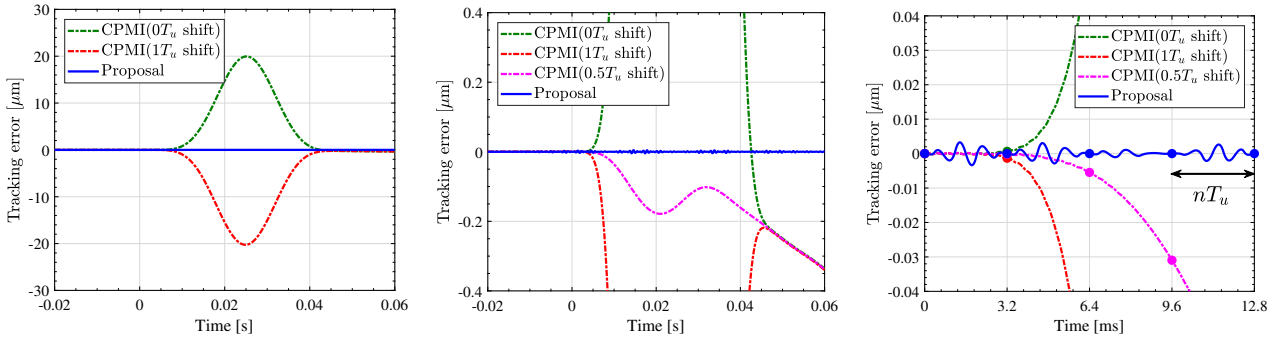

(a) Tracking error. (b) Tracking error (zoom). (c) Tracking error (zoom2).

Fig. 11. Error comparison between the proposed method and shifted CPMI method. Dots are illustrated by every $T_r = nT_u$. It shows that the proposed method achieves the perfect tracking for $T_r = nT_u$, which is not achievable by the CPMI method (simulation).

VI. Conclusion

In the discretized domain, there are two types of zeros: 1) the intrinsic zeros which have counterparts in the continuous time domain, 2) the discretization zeros generated by discretization by the zero-order hold. The proposed preactuated multirate feedforward control deals with problem 1) and 2) independently. On one hand, the unstable intrinsic zeros are compensated by the preactuation. On the other hand, the unstable discretization zeros are compensated by the multirate feedforward control with preview. Multirate feedforward controller generates the feedforward input, which achieves perfect tracking for the designed state trajectory. The simulation results show that the zero-order hold delay cannot be compensated by just shifting the reference and underline the importance of multirate feedforward.

This study experimentally validates the proposed method using a high-precision positioning stage with continuous time unstable zeros. Additionally, this system has a discretization zero. Owing to a well-identified 8th order model, the experimental results follow the simulations. The experimental result obtained with the proposed method strongly reduces the tracking error and achieves almost zero undershoot and overshoot.

Acknowledgment

This work is supported by JSPS KAKENHI Grant Number 18H05902.

References

[1] K. L. Moore, S. P. Bhattacharyya, and M. Dahleh, "Capabilities and limitations of multirate control schemes," *Automatica*, vol. 29, no. 4, pp. 941–951, 1993.

[2] T. Hagiwara, T. Yuasa, and M. Araki, "Stability of the limiting zeros of sampled-data systems with zero-and first-order holds," *International Journal of Control*, vol. 58, no. 6, pp. 1325–1346, 1993.

[3] T. Hagiwara, "Analytic study on the intrinsic zeros of sampled-data systems," *IEEE Transactions on Automatic Control*, vol. 41, no. 2, pp. 261–263, 1996.

[4] K. Åström, P. Hagander, and J. Sternby, "Zeros of sampled systems," *Automatica*, vol. 20, no. 1, pp. 31–38, 1984.

[5] H. Butler, "Position Control in Lithographic Equipment," *IEEE Control Systems Magazine*, vol. 31, no. 5, pp. 28–47, 2011.

[6] A. Hara, K. Saiki, K. Sakata, and H. Fujimoto, "Basic examination on simultaneous optimization of mechanism and control for high precision single axis stage and experimental verification," in *34th Annual Conference of IEEE Industrial Electronics*, pp. 2509–2514, 2008.

[7] K. Saiki, A. Hara, K. Sakata, and H. Fujimoto, "A Study on High-Speed and High-Precision Tracking Control of Large-Scale Stage Using Perfect Tracking Control Method Based on Multirate Feedforward Control," *IEEE Transactions on Industrial Electronics*, vol. 57, no. 4, pp. 1393–1400, 2010.

[8] H. Fujimoto, K. Fukushima, and S. Nakagawa, "Vibration suppression short-span seeking of HDD with multirate feedforward control," in *American Control Conference*, pp. 582–587, 2006.

[9] R. W. Erickson and D. Maksimovic, *Fundamentals of Power Electronics*. Springer, 2011.

[10] T. Miyajima, H. Fujimoto, and M. Fujitsuna, "A Precise Model-Based Design of Voltage Phase Controller for IPMSM," *IEEE Transactions on Power Electronics*, vol. 28, no. 12, pp. 5655–5664, 2013.

[11] G. Oriolo, A. D. Luca, and M. Vendittelli, "WMR control via dynamic feedback linearization: design, implementation, and experimental validation," *IEEE Transactions on Control Systems Technology*, vol. 10, no. 6, pp. 835–852, 2002.

[12] R. Stengel, *Flight Dynamics*. Princeton University Press, 2004.

[13] B. Rigney, L. Y. Pao, and D. Lawrence, "Nonminimum phase dynamic inversion for settle time applications," *IEEE Transactions on Control Systems Technology*, vol. 17, no. 5, pp. 989–1005, 2009.

[14] J. A. Butterworth, L. Y. Pao, and D. Y. Abramovitch, "Analysis and comparison of three discrete-time feedforward model-inverse control techniques for nonminimum-phase systems," *Mechatronics*, vol. 22, no. 5, pp. 577–587, 2012.

[15] J. Wen and B. Potsaid, "An experimental study of a high performance motion control system," in *American Control Conference*, vol. 6, pp. 5158–5163, 2004.

[16] M. Tomizuka, "Zero phase error tracking algorithm for digital control," *Journal of Dynamic Systems, Measurement, and Control*, vol. 109, pp. 65–68, 1987.

[17] L. Hunt, G. Meyer, and R. Su, "Noncausal inverses for linear systems," *IEEE Transactions on Automatic Control*, vol. 41, no. 4, pp. 608–611, 1996.

[18] S. Devasia, D. Chen, and B. Paden, "Nonlinear inversion-based output tracking," *IEEE Transactions on Automatic Control*, vol. 41, no. 7, pp. 930–942, 1996.

[19] L. Biagiotti and C. Melchiorri, *Trajectory Planning for Automatic Machines and Robots*, Springer, 2008.

[20] T. Shiraishi and H. Fujimoto, "A Reference Trajectory Generation for System with Unstable Zeros Considering Negative-time Domain Analysis," in *IEEJ International Workshop on Sensing, Actuation, and Motion Control*, 2015.

[21] L. Marconi, G. Marro, and C. Melchiorri, "A solution technique for almost perfect tracking of non-minimum-phase, discrete-time linear systems," *International Journal of Control*, vol. 74, no. 5, pp. 496–506, 2001.

[22] T. Sogo and M. Joo, "Design of Compensators to Relocate Sampling Zeros of Digital Control Systems for DC Motors," *SICE Journal of Control, Measurement, and System Integration*, vol. 5, no. 5, pp. 283–289, 2012.

[23] J. van Zundert and T. Oomen, "Stable inversion of LPTV systems with application in position-dependent and non-equidistantly sampled systems," *International Journal of Control*, pp. 1–11, 2017.

[24] L. Blanken, G. Isil, S. Koekebakker, and T. Oomen, "Flexible ILC:

towards a convex approach for non-causal rational basis functions," *IFAC-PapersOnLine*, vol. 50, no. 1, pp. 12 107–12 112, 2017.
[25] W. Ohnishi and H. Fujimoto, "Multirate Feedforward Control with State Trajectory Generation based on Time Axis Reversal for Plant with Continuous Time Unstable Zeros," in *IEEE International Conference on Advanced Intelligent Mechatronics*, pp. 689–694, 2016.
[26] W. Ohnishi, T. Beauduin, and H. Fujimoto, "Preactuated multirate feedforward for a high-precision stage with continuous time unstable zeros," *IFAC-PapersOnLine*, vol. 50, no. 1, pp. 10 907–10 912, 2017.
[27] H. Fujimoto, Y. Hori, and A. Kawamura, "Perfect tracking control based on multirate feedforward control with generalized sampling periods," *IEEE Transactions on Industrial Electronics*, vol. 48, no. 3, pp. 636–644, 2001.
[28] S. Bittanti, F. Dell'Orto, A. Di Carlo, and S. M. Savaresi, "Notch filtering and multirate control for radial tracking in high-speed DVD-players," *IEEE Transactions on Consumer Electronics*, vol. 48, no. 1, pp. 56–62, 2002.
[29] T. Atsumi and W. Messner, "Compensating for ZOH-Induced Residual Vibrations in Head-Positioning Control of Hard Disk Drives," vol. 19, no. 1, pp. 258–268, 2014.
[30] J. van Zundert and T. Oomen, "LPTV Loop-Shaping with Application to Non-Equidistantly Sampled Precision Mechatronics," *Proceedings of 15th International Workshop on Advanced Motion Control*, pp. 467–472, 2018.
[31] H. Fujimoto and B. Yao, "Multirate adaptive robust control for discrete-time non-minimum phase systems and application to linear motors," *IEEE/ASME Transactions on Mechatronics*, vol. 10, no. 4, pp. 371–377, 2005.
[32] T. Chen and B. A. Francis, *Optimal Sampled-Data Control Systems*, Springer, 1995.
[33] G. C. Goodwin, S. F. Graebe, and M. E. Salgado, *Control System Design*, Prentice Hall, 2000.
[34] T. Sogo, "On the equivalence between stable inversion for nonminimum phase systems and reciprocal transfer functions defined by the two-sided Laplace transform," *Automatica*, vol. 46, no. 1, pp. 122–126, 2010.
[35] R. Pintelon, P. Guillaume, Y. Rolain, J. Schoukens, and H. Van Hamme, "Parametric identification of transfer functions in the frequency domain-a survey," *IEEE Transactions on Automatic Control*, vol. 39, no. 11, pp. 2245–2260, 1994.
[36] W. Ohnishi, T. Beauduin, and H. Fujimoto, "Finite Time Optimal Preactuation for Non-Minimum Phase Systems Considering Control Input and Tracking Error Constraints," in *IEEE Conference on Control Technology and Applications*, pp. 1114–1119, 2018.

Wataru Ohnishi received the B.E., M.S., and Ph.D. degrees from the University of Tokyo, Japan in 2013, 2015, and 2018, respectively.

Presently, he is a research associate with the Department of Electrical Engineering and Information Systems, Graduate School of Engineering, the University of Tokyo. His research interest includes high-precision motion control. He is a member of the Institute of Electrical Engineers of Japan.

Thomas Beauduin received the B.S. and M.S. degrees in Mechanical Engineering from the University of Leuven in 2012 and 2014, respectively. In 2014, he joined Hori-Fujimoto laboratory as a research assistant in the Department of Electrical Engineering and Information Systems at the University of Tokyo, Japan. Since 2017, he has been working as a research engineer for MTT, a startup company from the Department of Computer Science at the University of British Columbia, Canada. His research interests include nano-scale motion control and optics.

Hiroshi Fujimoto received the Ph.D. degree in the Department of Electrical Engineering from the University of Tokyo in 2001. In 2001, he joined the Department of Electrical Engineering, Nagaoka University of Technology, Niigata, Japan, as a research associate. From 2002 to 2003, he was a visiting scholar in the School of Mechanical Engineering, Purdue University, U.S.A. In 2004, he joined the Department of Electrical and Computer Engineering, Yokohama National University, Yokohama, Japan, as a lecturer and he became an associate professor in 2005. He is currently an associate professor of the University of Tokyo since 2010. He received the Best Paper Award from the IEEE Transactions on Industrial Electronics in 2001 and 2013, Isao Takahashi Power Electronics Award in 2010, Best Author Prize of SICE in 2010, and The Grand Nagamori Award in 2016. His interests include control engineering, motion control, nano-scale servo systems, electric vehicle control, and motor drive. Dr. Fujimoto is a member of IEEE, the Society of Instrument and Control Engineers, the Robotics Society of Japan, and the Society of Automotive Engineers of Japan.